

Tunable plasmon excitations and electron conductivity in irradiated $\alpha - \mathcal{T}_3$ materials

Andrii Iurov^{1*}, Liubov Zhemchuzhna², Dipendra Dahal², Godfrey Gumbs^{2,3}, and Danhong Huang^{4,1}

¹*Center for High Technology Materials, University of New Mexico,
1313 Goddard SE, Albuquerque, New Mexico, 87106, USA*

²*Department of Physics and Astronomy, Hunter College of the City University of New York,
695 Park Avenue, New York, New York 10065, USA*

³*Donostia International Physics Center (DIPC),
P de Manuel Lardizabal, 4, 20018 San Sebastian, Basque Country, Spain*

⁴*Air Force Research Laboratory, Space Vehicles Directorate,
Kirtland Air Force Base, New Mexico 87117, USA*

(Dated: December 15, 2024)

In the presence of external off-resonance circularly polarized irradiation, we have performed a detailed numerical analysis of the dynamic polarizability in α - \mathcal{T}_3 lattices. This is then employed in calculations of plasmon dispersions and their damping, optical and Boltzmann conductivities for various values of the material parameter α . Both the collective excitations and transport properties show strong dependence on α , especially approaching the graphene limit when $\alpha \rightarrow 0$, and may also be slightly tuned by the dressing field. The frequency of the plasmon modes could be increased, whereas the transport conductivity shows a noticeable decrease, due to the applied irradiation. These properties should be useful in the construction of novel nano-electronic and nano-plasmonic devices.

I. INTRODUCTION

Currently, the $\alpha - \mathcal{T}_3$ model seems to present prospective opportunities for revolutionizing low-dimensional physics through novel two-dimensional (2D) materials.¹ Its atomic configuration consists of a graphene-type honeycomb lattice along with an additional site, i.e., a hub atom at the center of each hexagon.² An essential material parameter $\alpha = \tan \phi$, which enters into its low-energy Dirac-Weyl pseudospin-1 Hamiltonian, represents the ratio between the rim-to-hub and rim-to-rim hopping coefficients. This parameter affects all fundamental electronic properties of the lattice. It is believed to vary from 0 to 1 for different types of $\alpha - \mathcal{T}_3$ materials, which may lead to some important technological applications in electronic devices. The case when $\alpha = 0$ corresponds to graphene with a completely separated flat band, whereas when $\alpha = 1$, we have the pseudospin-1 dice lattice, which has been fabricated and studied considerably.^{3,4} Consequently, the $\alpha - \mathcal{T}_3$ model may be regarded as an interpolation between graphene and the dice lattice, or pseudospin-1 \mathcal{T}_3 model. Its low-energy dispersion consists of a cone, which is similar to that for graphene,⁵ and a flat band with zero-energy separating the valence from the conduction band for these pseudospin-1 materials.^{6,7}

In recent times, there have been numerous attempts leading to an actual experimental realization of the $\alpha - \mathcal{T}_3$ model. Its topological characteristics, comprising a Dirac cone with three bands located at a single point, were exhibited in the triplon band structure of $SrCu_2(BO_3)_2$, which is an example of a Mott-Hubbard insulator.⁸ Dielectric photonic crystals with zero refractive index have Dirac cone dispersion at the center of the Brillouin zone in the presence of an accidental degeneracy.^{9,10} Most importantly, there are various types of photonic Lieb lattices^{11,12} consisting of a 2D array of optical waveguides. Such structure demonstrate a three-band structure, which includes a perfectly flat middle band.

Further to a relatively recent discovery of $\alpha - \mathcal{T}_3$, there have been a few crucial publications devoted to investigating their magnetic,^{1,13–15} optical,^{16,17} many-body⁷ and electron transport properties,^{18,19} as well as generalized versions of the model.²⁰ A number of compelling properties of graphene and other low-dimensional materials²¹ have also been investigated in $\alpha - \mathcal{T}_3$, including Klein tunneling^{22,23} and the Hofstadter butterfly.²⁴ On the other hand, all pseudospin-1 structures display some previously unobserved phenomena, originating from the presence of the flat band in its energy dispersion,²⁵ for example, very specific plasmons with branch “pinching” at the Fermi level.⁷

We note that an exciting emergent technical application for condensed matter quantum optics, is *Floquet engineering*. This has wide-range optical tuning capability and control of the electronic behavior and transport in 2D

* E-mail contact: aiurov@unm.edu, theorist.physics@gmail.com, webpage: https://www.researchgate.net/profile/Andrii_Iurov

materials by applying off-resonant periodic dressing field in the terahertz or microwave range.^{26–32} Such external irradiation imposed on a 2D material leads to a dramatic change in most of its electronic properties due to creating so-called *dressed states*. This defines a single quantum object, consisting of an electron interacting with a photon. It is described by modified energy dispersion relations, which now depend on the intensity and polarization of the incoming radiation.

Our investigation of the electron dressed states is based on Floquet theory of quantum systems, driven by external periodic potentials. This results in various $\sim 1/(\hbar\omega)$ series expansions, such as for Floquet-Magnus, Brillouin-Wigner and others,³³ playing an essential role in the investigation of the electron-light interaction in a variety of novel 2D materials^{34–37} and optically induced topological surface states.³⁸

The modification of the single-particle dispersion relations as well as basic electronic properties strongly affects the many-body properties^{21,39,40} in addition to the electronic transport,^{41,42} specifically, the Boltzmann conductivity.⁴³ This is due mainly due to the opening of an energy bandgap³⁴ between the valence and conduction bands, and the corresponding change in the electronic wave functions.⁴⁴ For the case of linearly-polarized dressing field, we observe strong in-plane anisotropy, while initially anisotropic dispersion relations in phosphorene also undergo significant variations.⁴⁵

Once Floquet engineering is applied to $\alpha - \mathcal{T}_3$ materials, we will be impressed by the counter-intuitive findings, such as anisotropy, opening inequivalent energy band gaps within each band, breaking of the electron-hole symmetry and valley degeneracy,¹⁶ significant variations of the electron wave function, their symmetries and the Berry phases.⁴⁶ Specifically, applying circularly-polarized light induces a topological phase transition from a gapless semimetal to a topological insulator with a non-zero Chern number.¹⁷ This has some resemblance with a topological insulator, obtained from a periodic array of quantum rings under circularly-polarized light field.⁴⁷

II. ELECTRON DRESSED STATES IN $\alpha - \mathcal{T}_3$ MODEL

In the presence of an external field, the single-electron states are obtained by making the following replacement for the wave vector components $k_{x,y} \rightarrow k_{x,y} - e/\hbar A_{x,y}^{(C)}(t)$ in the low-energy Hamiltonian of the considered material. In this notation, $\mathbf{A}^{(C)}(t)$ is the vector potential of the applied circularly polarized field. Therefore, the resulting Hamiltonian experiences an additional time-dependent term, corresponding to the electron-light interaction. In this paper, we deal with circular polarization of the dressing field so that $\mathbf{A}^{(C)}(t) = \mathcal{E}/\omega \{\cos(\omega t), \sin(\omega t)\}^T$ with the two equal and $\pi/2$ phase-shifted components. Here, \mathcal{E} is the amplitude of the electric field of the imposed radiation and ω is its frequency in off-resonance regime.

We have used Floquet-Magnus perturbation expansion theory. This procedure is applicable to any periodically driven quantum structure,³³ to obtain valley-degenerate, isotropic and symmetric near the flat energy band structure.⁴⁶ This is given by $\varepsilon_d(\mathbf{k}) = 0$ and

$$\varepsilon_d(\mathbf{k}) = \pm \sqrt{(\lambda_0 c_0/4)^2 + [\hbar v_F k (1 + \lambda_0^2/4)]^2}, \quad (1)$$

where $c_0 = v_F e \mathcal{E}/\omega$ is the interaction coefficient (energy), and $\lambda_0 = c_0/(\hbar\omega) = v_F e \mathcal{E}/(\hbar\omega^2)$ is a dimensionless electron-light coupling parameter. Since our consideration is limited within the off-resonance frequencies of the dressing field, in which the photon energy greatly exceeds any of the representative electron energies of the material, such as Fermi energy E_F , $\lambda_0 \ll 1$ disregarding of the actual light intensity $\mathbb{I} = \epsilon_0 c \mathcal{E}^2/2 \sim 10 \text{ W/cm}^2$.

These dispersions reveal an energy band gap $\varepsilon_G = 2\Delta_0 = \lambda_0 c_0/2$, which is *twice as small as* the corresponding gap in graphene with the same interaction coefficient c_0 ³⁴.

$$\Psi_d^{(C)}(\gamma, \tau | \lambda_0, \mathbf{k}) = \frac{1}{\sqrt{\mathcal{N}(\gamma)}} \begin{Bmatrix} \tau \mathcal{C}^{(1)} \mathbf{e}^{-i\tau\theta_{\mathbf{k}}} \\ \mathcal{C}^{(2)} \\ \tau (\hbar v_F k)^2 \mathbf{e}^{+i\tau\theta_{\mathbf{k}}} \end{Bmatrix}, \quad (2)$$

where

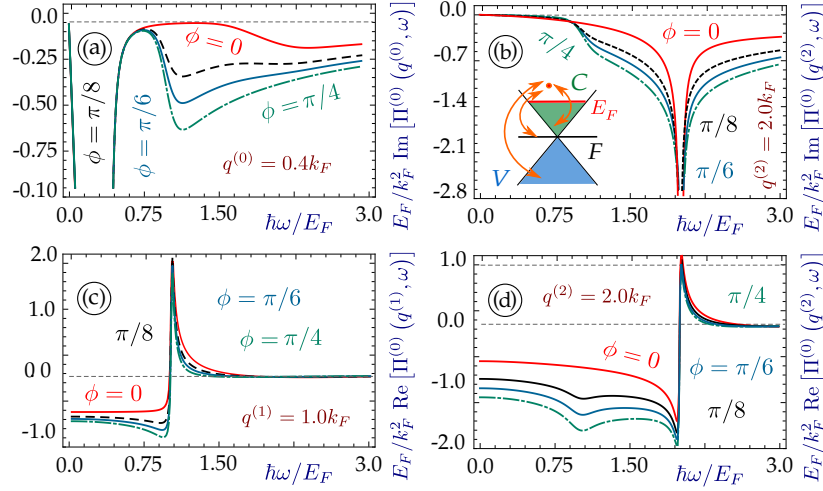


FIG. 1: (Color online) Frequency (ω) and wave vector (q)-dependent polarization function $\Pi^{(0)}(q, \omega | \phi, \lambda_0 = 0)$ (in units of k_F^2/E_F) for non-irradiated $\alpha - \mathcal{T}_3$ model as a function of frequency, for various values of the phase ϕ . Each panel corresponds to chosen wave vector $q^{(i)}$ and each curve to a specific phase ϕ , as labeled. The two upper panels (a) and (b) present the real part of $\Pi^{(0)}(q, \omega | \phi, \lambda_0 = 0)$, whereas the two lower ones (c) and (d) its imaginary part. The only inset on plot (b) is a schematics illustrating all possible single-particle transitions which contribute to the polarization function at $T=0$ K.

$$\begin{aligned} \mathcal{C}^{(1)}(\gamma, \tau | \lambda_0, k) &= (\hbar v_F k)^2 + 2 \left[\Delta_{(\lambda)}^2 - 2c_0 \lambda_0 \gamma \tau \sqrt{(\hbar v_F k)^2 + \Delta_{(\lambda)}^2} \right], \\ \mathcal{C}^{(2)}(\gamma, \tau | \lambda_0, k) &= \sqrt{2} \gamma (\hbar v_F k) \left[\sqrt{(\hbar v_F k)^2 + \Delta_{(\lambda)}^2} - \gamma \tau \Delta_{(\lambda)} \right], \\ \mathcal{N}^{(\gamma)}(\tau | \lambda_0 \ll 1, k) &\simeq 2 \left\{ 2 (\hbar v_F k)^4 - 5 \gamma \tau c_0 \lambda_0 (\hbar v_F k)^3 + 9 [c_0 \lambda_0 (\hbar v_F k)]^2 \right\}. \end{aligned} \quad (3)$$

The parameter $\Delta_{(\lambda)} = 2\lambda_0 c_0 / (4 + \lambda_0^2)$ is not equivalent to the actual energy bandgap $2\Delta_0(\beta = 1, \lambda_0) = \lambda_0 c_0$.

For the flat band, we obtain

$$\Psi_d^{(C)}(\gamma = 0, \tau | \lambda_0, \mathbf{k}) = \frac{1}{\sqrt{\mathcal{N}^{(0)}}} \left\{ \frac{k \mathbf{e}^{-i\tau\theta_{\mathbf{k}}}}{k \mathbf{e}^{+i\tau\theta_{\mathbf{k}}}} 2\sqrt{2} \lambda_0 (4 - \lambda_0^2) c_0 / (\hbar v_F) \right\}, \quad (4)$$

where

$$\mathcal{N}^{(0)}(\lambda_0 \ll 1, k) \simeq 2 \left[k^2 + \left(8\lambda_0 \frac{c_0}{\hbar v_F} \right)^2 \right] + \dots \quad (5)$$

The obtained electronic states are specifically related to an irradiated dice material and not equivalent to those derived by adding a $\Delta_0 \hat{\Sigma}_z^{(3)}$ gap-generating Hamiltonian term ($\hat{\Sigma}^{(3)}$ is a three-dimensional z -Pauli matrix with the main diagonal $\{1, 0, -1\}$), used to describe the effect of a point defect. ²⁵

III. POLARIZATION FUNCTION AND PLASMONS

The self-sustaining charge density oscillations, i.e., plasmons play an important role in determining the optical properties of low-dimensional structures. ^{21,44,48-50} These include exotic fullerenes and spherical graphitic particles. ⁵¹⁻⁵³

The plasmon dispersion relations in the wave vector-frequency (q, ω)-plane () correspond to the zeros of the dielectric function $\epsilon(q, \omega)$, which is expressed in terms of the dynamical polarization function as $\epsilon(q, \omega) = 1 - 2\pi\alpha_\epsilon/q \Pi^{(0)}(q, \omega)$.

In this notation, $\alpha_\epsilon = e^2/(4\pi\epsilon_0\epsilon_r)$ is the inverse dielectric constant, determined by the substrate material with background dielectric constant ϵ_r . The dynamical polarizability is also involved in determining impurity shielding. The screened potential for a dilute distribution of impurities embedded in a dice lattice has been investigated⁷ as well as for a general type of $\alpha - \mathcal{T}_3$.⁵⁴ Furthermore, the polarizability of any $\alpha - \mathcal{T}_3$ lattice at $T=0$ K may be substantially differs from that for graphene as shown in Fig. 1. This is due to the additional electron transitions from the flat band, as depicted in the inset in Fig. 1(b), especially for frequencies near the Fermi level.

The particle-hole continuum comprising the single-particle excitation regions are defined as the regions with finite imaginary part of the polarization function. Once a plasmon branch enters such a region, there is Landau damping resulting in the decay of a plasmon into single-particle excitations. Thus, we are interested in finding the regions of long-lived plasmons with $\text{Im} [\Pi^{(0)}(q, \omega)] = 0$, which are free from Landau damping.

In our calculations, we scan (q, ω) space where the plasmons could possibly exist. We find that for all $\alpha - \mathcal{T}_3$ materials, there is one *triangle* region below the Fermi level E_F and another above the main diagonal $\omega = v_F q$, as shown in Fig. 2. Here, v_F is the Fermi velocity. Even though there are additional areas free from Landau damping for $q > 2k_F$, where k_F is the Fermi wave vector, plasmon branches in free-standing 2D materials cannot be located there. Strictly speaking, the plasmon begins to decay once the branch enters the region above $\omega = E_F$, however the strength of this damping varies for ϕ and becomes infinitesimally small and eventually disappears for graphene with $\phi \rightarrow 0$.

Our results for the polarizability at $T = 0$ K for finite hopping parameter satisfying the condition $0 < \alpha < 1$ (or $0 < \phi < \pi/4$) are presented in Figs. 1(a) through 1(d). Its imaginary part shows a noticeable increase at low energies, compared with graphene in Fig. 1(a). At large wave vectors $q \geq k_F$, there is a single infinite pole $\sim -|q^2 - \omega^2|^{-1/2}$, just it was previously demonstrated for graphene referring to Fig. 1(b). Similar behavior for the real part of the polarizability is noticed in Fig. 1(c), which also shows an additional peak, which affects the location of a plasmon mode whose frequency in the chosen range is determined by the plot in Fig. 1(d).

Plasmon energy essentially determines at what extent each branch is affected by the electron transitions from and to the flat band. The presence of this additional band is most apparent next to the Fermi level E_F , where various plasmon branches with different α_ϵ in a dice lattice are pinched at a single point $\hbar\omega = E_F = \hbar v_F q$.⁷ We have noticed that for an intermediate case of $\phi = \pi/6$ such plasmon branches still demonstrate two different peaks of their separation from the diagonal $\hbar v_F q$ below and above E_F , but no actual pinching occurs - all the branches cross the $\hbar\omega = E_F$ energy level at different wave vectors q (see Fig. 2 (c)).

An interesting result was extracted by analyzing the degree to which a plasmon mode, corresponding to a chosen phase ϕ , is separated from the boundary of single-particle excitations $\hbar v_F q$. For all $\alpha - \mathcal{T}_3$ materials, the plasmon modes are located below those in graphene ($\phi = 0$, red line in Fig. 2(d)). For each chosen ϕ , there are a pair of plasmon branches corresponding to two clearly well-defined loss peaks depicting their "distance" from $\hbar v_F q$, except for $\phi = 0$. The undamped part of each branch when $\hbar\omega < E_F$ spans a much larger (up to $\times 10$) range of the wave vector q compared to the case of graphene. Except for their dispersion near E_F , all the plasmon curves show quite similar behavior in the long wavelength limit $q \ll E_F/(\hbar v_F)$, corresponding to the short-range electron transitions across the Fermi level, and for the frequencies much above the Fermi energy, related to the far-inter-cone transitions with large energy and momentum transfer.

In summary, we believe that the best opportunity for observing the ϕ -, or α -dependence of the plasmon dispersions and damping occurs when $\phi \simeq 0$, i.e., in the vicinity of the graphene limit. This is so because the results for $\phi = \pi/6$ and dice show only little difference as can be seen by comparing Figs. 2(a) and 2(b)). In accordance with the trigonometric expression for the main Hamiltonian terms of $\alpha - \mathcal{T}_3$, qualitatively, such dependence could be presented as $\sim \cos(2\phi)$.

Next, we turn our attention to the dependence of the polarizability and plasmon dispersion of $\alpha - \mathcal{T}_3$ materials on circularly-polarized irradiation. Specifically, we focus on a dice lattice, which is the most diverse from graphene. In graphene, the effect of circularly-polarized is almost equivalent to opening a gap via adding a $\hat{\sigma}_z^{(2)}$ term to the initial Dirac Hamiltonian.⁴⁴ The most important difference for the dice lattice, and for all $\alpha > 0$, is that its static polarizability $\Pi^{(0)}(q, \omega = 0)$ is not constant for $q < 2k_F$ (see Fig. 3 (a)). At the same time, applying the irradiation leads to a certain reduction of the static polarization function.

The static screening factor $|1/\epsilon(q, \omega = 0 | \lambda_0)|^2$, shown in the inset (i1) of Fig. 3, is a fundamental component in evaluating the Boltzmann conductivity. It is found to be strongly affected by the irradiation, even if the coupling λ_0 is weak, its ratio between the non-irradiated material and with $\lambda_0 = 0.5$, is nearly twice. In the presence of finite electron-light coupling λ_0 , the peaks of the imaginary part of the polarizability are shifted towards higher frequencies, while its real part undergoes a completely opposite change (compare panels (b) and (c) of Fig. 3).

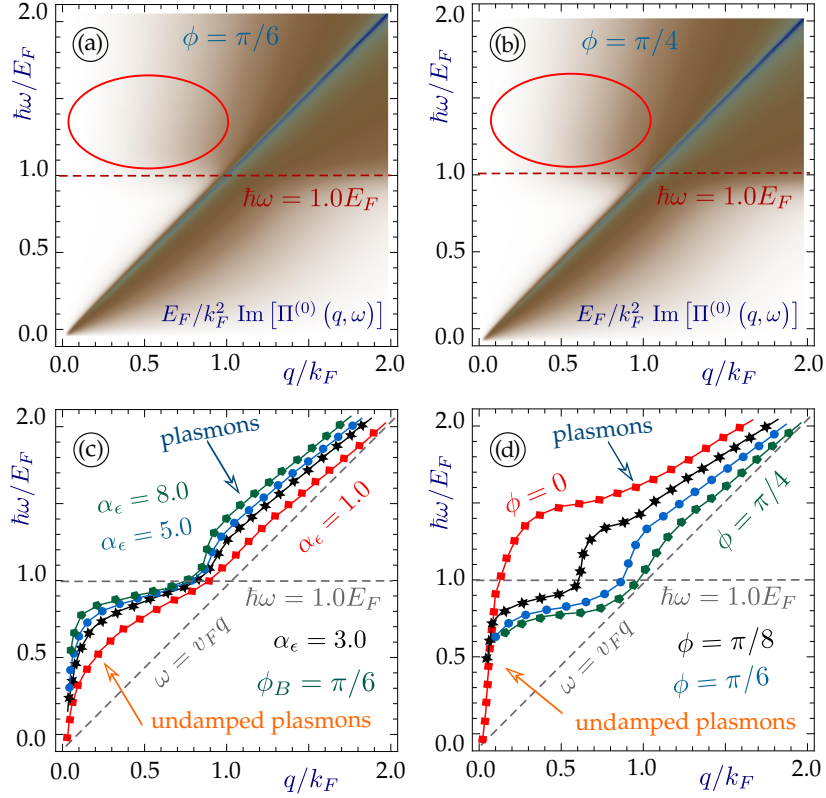


FIG. 2: (Color online) Plasmon damping regions (upper panels (a) and (b)) and branches ((c) and (d)) for various types of $\alpha - \mathcal{T}_3$ lattices in the absence of external irradiation. The upper plots in (a) and (b) show $\text{Im}[\Pi^{(0)}(q, \omega | \phi, \lambda_0 = 0)]$, which represents the single-particle excitation regions. Panel (c) presents the plasmon dispersion relations for a material with $\phi = \pi/6$ and different values of the inverse dielectric constant α_ϵ , and (d) shows the plasmon modes for $\alpha - \mathcal{T}_3$ lattices with chosen phase $\phi = \tan^{-1} \alpha$, for each branch, and $\alpha_\epsilon = 3.0$.

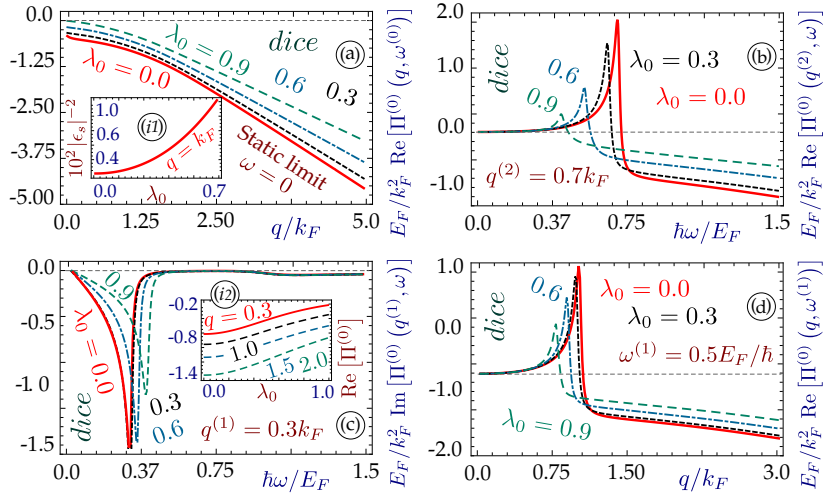


FIG. 3: (Color online) The zero-temperature polarization function $\Pi^{(0)}(q, \omega | \phi, \lambda_0)$ (in units of k_F^2/E_F) for a dice lattice under external circularly polarized dressing field with various electron-light coupling constants λ_0 . All panels, except for (c), and both insets show the real part of the polarizability. Two plots (a) and (d) demonstrate the frequency dependence of $\Pi^{(0)}$ for a fixed wave vector $q^{(i)}$, and the two remaining panels (b) and (c) show the opposite case of a wave vector dependence for a specific frequency. In all panels, each curve corresponds to a chosen value of coupling λ_0 , as labeled. Panel (a) and both insets are concerned with the static limit $\omega = 0$.

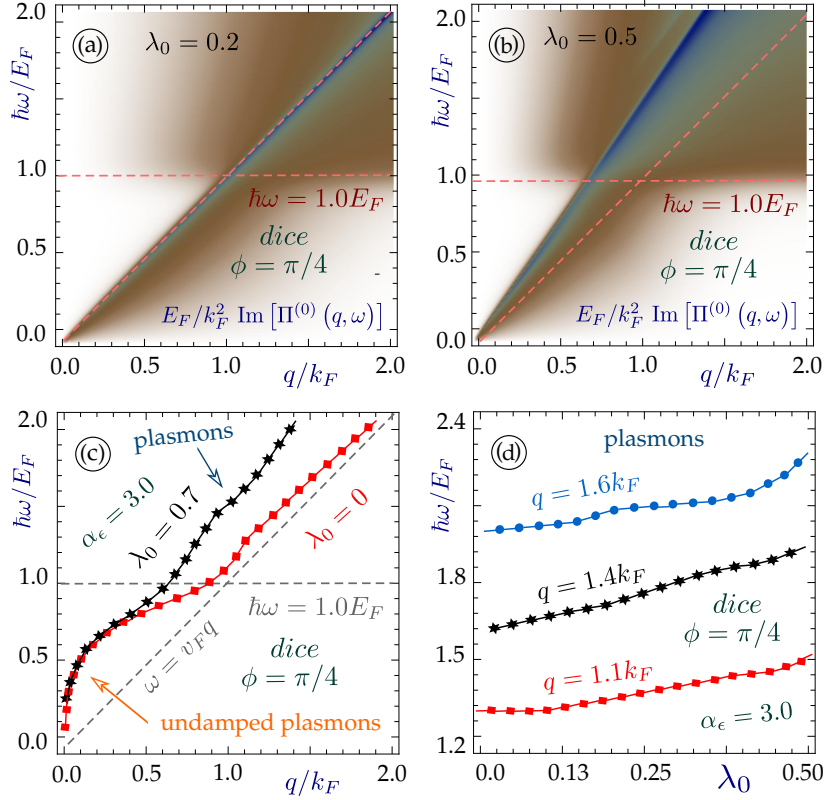


FIG. 4: (Color online) Panels (a) and (b) show $\text{Im}[\Pi^{(0)}(q, \omega | \phi, \lambda_0 \neq 0)]$ for regions where plasmons are Landau damped. Panels (c) and (d) present the plasmon dispersion relations. The results are for a dice lattice under an external dressing field with different electron-light coupling parameters λ_0 .

In general, we often observe that the increase of the phase ϕ from graphene to a dice lattice and the presence of a dressing field lead to opposite and conflicting effects. Specifically, in the static limit, finite dressing results in a drop of the polarization. Since the actual effects of external irradiation in off-resonance regime is significantly smaller than any change of α , the obtained results provide a unique possibility for fine-tuning of all crucial electronic properties, including the conductivity, in all $\alpha - \mathcal{T}_3$ materials.

For an irradiated material, very strong Landau damping is present above the main $\hbar v_F q$, as we show at Fig. 4(b). This affects the frequency range of long-lived plasmon excitations compared with $\lambda_0 = 0$. Our results for the plasmon dispersion presented in Figs. 4(c) and 4(d), demonstrate a totally unexpected robust increase of their frequency due to the radiation. This reveals a fundamental difference with the plasmon dispersions in graphene, which have a lowered frequency $\sim 1 - (\Delta_0^G/E_F)^2$, $\Delta_0^G = \lambda_0 c_0$. The reason for this is attributed to the presence of a flat band, which substantially changes both real and imaginary parts of the polarization function, and the fact that the energy gap is now twice as small. We also cannot detect a finite separation between the intra- and inter-band parts of the single-particle excitation regions since the plasmon mode is always damped for $\omega > E_F/\hbar$, corresponding to the electron transition, related to the flat band.

IV. TRANSPORT PROPERTIES

Our formalism for calculating the conductivity of interacting electrons is based on the polarization function, which we discussed above. Specifically, the optical conductivity $\sigma_O(\lambda_0, \omega)$ is directly proportional to its long wave limit as $\sigma_O(\lambda_0, \omega) = \lim_{q \rightarrow 0} \{ie^2 \omega/q^2 \Pi(q, \omega | \lambda_0)\}$. The real or absorptive part of σ_O corresponds to the imaginary part of the polarizability.

Our results for the optical conductivity, presented in Fig. 5, show that its peak appearing just above the Fermi energy is estimated for graphene as $\simeq 1 + \{2\Delta_0^G/(\hbar\omega)\}^2$. This is higher than a flat constant portion, corresponding

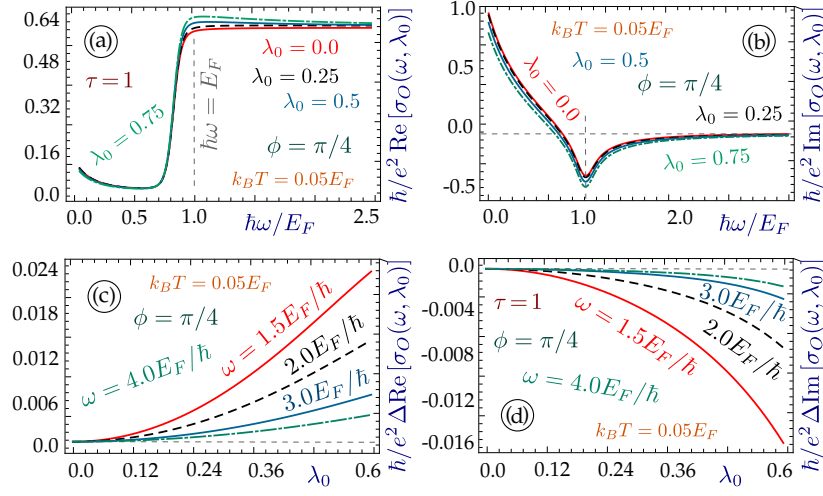


FIG. 5: (Color online) Optical conductivity $\sigma_O(\omega, \lambda_0)$ (in units of e^2/\hbar) for an irradiated dice lattice with different electron-light coupling parameters λ_0 . The two upper panels (a) and (b) present the frequency dependence of $\sigma_O(\omega, \lambda_0)$ for $\lambda_0 = 0.0, 0.25, 0.5$ and 0.75 , as labeled. The lower panels (c) and (d) show the variation of the optical conductivity as a function of λ_0 for chosen frequency ω . Both left plots (a) and (c) represent the real, or absorptive, part of $\sigma_O(\omega, \lambda_0)$, while the panels on the right-hand-side its imaginary part.

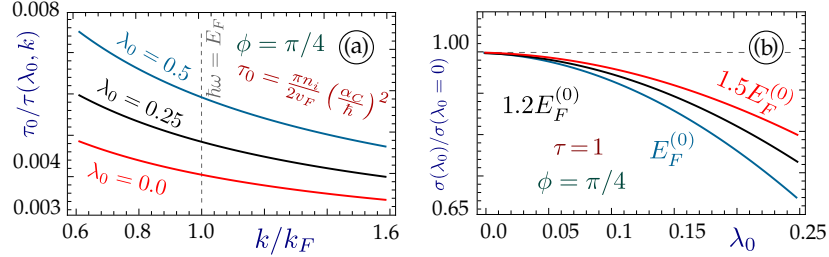


FIG. 6: (Color online) Boltzmann conductivity for the irradiated dice lattice. Panel (a) presents the inverse relaxation time, obtained from Eq. (6), as a function of wave vector k for various electron-light coupling constant λ_0 . Plot (b) shows the conductivity as a function of the dressing field (ratio of σ_λ to σ_0 which is the conductivity in the absence of irradiation) as a function of λ_0 .

to a gapless Dirac cone,^{55,56} which is now observed for much wider frequency ranges. Similarly, the imaginary part of σ_O shows a steady difference due to the irradiation for all allowable frequencies. The λ_0 dependence, presented in Figs. 5(c) and 5(d) is decreased for the larger ω , similarly to the polarizability and plasmon dispersion.

Finally, we consider the *Boltzmann conductivity* of an irradiated dice lattice. We calculated the conductivity in the relaxation time approximation, while the scattering potential is equivalent to the Coulomb interaction with a charged impurity $Q - U_C(\mathbf{r}) = eQ/(4\pi\epsilon\epsilon_0 r)$. For finite electron doping $E_F > 0$, the inverse relaxation time is given by^{57–60}

$$\frac{1}{\tau(k, \lambda_0)} = \frac{n_i}{2\pi\hbar} \int_0^{2\pi} d\beta_{\mathbf{k}, \mathbf{k}'} (1 - \cos \beta_{\mathbf{k}, \mathbf{k}'}) \int_0^\infty k' dk' \left| \left\{ \int d^2\mathbf{r} \Psi(\mathbf{k}' | \mathbf{r}) U_C(\mathbf{r}) \Psi(\mathbf{k} | \mathbf{r}) \right\} / \epsilon^{(s)}(|\mathbf{k} - \mathbf{k}'|) \right|^2 \delta[\varepsilon(k) - \varepsilon(k')], \quad (6)$$

where $\theta_{\mathbf{k}, \mathbf{k}'}$ is the angle between \mathbf{k} and \mathbf{k}' , the complete wave function is $\Psi(\mathbf{k} | \mathbf{r}) = \Psi_d(\lambda_0, \mathbf{k}) \exp[i\mathbf{k} \cdot \mathbf{r}]$. For isotropic dispersions and electronic states, corresponding to the circularly-polarized irradiation, the relaxation time depends only on $k = |\mathbf{k}|$. In the absence of screening, the relaxation time could be easily obtained analytically as we have shown in our *Supplementary materials*.

For the isotropic case of circularly polarized irradiation, the only non-zero component of the electric current is directed along the applied field E_e and is expressed as

$$\mathbf{j} = \left(\frac{e}{\pi}\right)^2 \int d^2\mathbf{k} E_e [v_g(\lambda_0, k)]^2 \tau(\lambda_0, k) \delta[\varepsilon_d(k) - E_F]. \quad (7)$$

In this notation, the delta function $\delta[\varepsilon(k)_d - E_F]$ corresponds to the zero-temperature limit of the negative $d/d\varepsilon$ -derivative of the Fermi-Dirac distribution, and no integration is needed.

The relaxation time for a non-irradiated dice lattice is $3/4\times$ of that in graphene due to the difference in wave function overlap factor, which in the former case is equal to $(1 + \cos \beta_{\mathbf{k},\mathbf{k}'})^2/4$. Once the circularly polarized irradiation is applied, the inverse relaxation time is modified to be $\simeq 3\pi/4 + 3\pi/4 \xi - 37\pi/16 \xi^2 + \dots$, where $\xi = c_0 \lambda_0 / E_F = e\mathcal{E}/\{(\hbar\omega)^2 k_F\}$. This strong increase of the first order of $\sim \lambda_0 c_0 / E_F$ essentially determines the decrease in conductivity in the presence of light. Such an expansion could be obtained only for a pseudospin-1 wave function with three inequivalent components, but not for graphene or a 2D electron gas.

Another modification of the conductivity comes from the λ_0 -dependent variation of the electron group velocity $v_g(\lambda_0, k)$ in Eq. (7), given as $\{v_g(\lambda_0, k)/v_F\}^2 \simeq (1 + \lambda_0^2/4)^2 \{1 - \lambda_0^2/4 (c_0/E_F)^2\}$. The two terms are related to the modification of the slope of the Dirac cone in the dispersion in Eq. (1) and to the opening of a band gap, and in fact have a conflicting effect on the conductivity. The ratio $\sigma_B(\lambda_0)/\sigma_B(\lambda_0 = 0)$ depends on the intensity of the irradiation. For normally used $I = 10 \text{ W/cm}^2$, $c_0/E_F \simeq 9.75$ there is always a decrease.

These results are quite different from graphene, in which the square of the group velocity is decreased as $\sim 1 - (\Delta_0^G/E_F)^2$, and the relaxation time is also reduced according to $\sim 1 - 3(\Delta_0^G/E_F)^2$,⁴³ i.e., both contributions work together to lower the Boltzmann conductivity. The same goes for the screening, which is also reduced and must be taken into account for an accurate determination of $\sigma_B(\lambda)$.

Our numerical results for the inverse relaxation time and the conductivity when the screening factor $1/|\epsilon(q, \omega = 0)|^2$ is taken into account are presented in Fig. 6. Even though the dependence on k and λ_0 qualitatively agrees with our analytical approximations, the actual results differ quite a lot, since the static dielectric constant is correlated with λ_0 substantially, as we showed in the inset of Fig. 3.

V. CONCLUDING REMARKS AND SUMMARY

In this paper, we have obtained and analyzed theoretical results for plasmon dispersion relations, their Landau damping, as well as the optical and Boltzmann conductivities in various $\alpha - \mathcal{T}_3$ lattices with $0 \leq \alpha \leq 1$. For the dice lattice, we analyzed the way in which all these properties are modified in the presence of circularly-polarized off-resonance dressing fields. As a consequence, we propose two different types of tuning of the collective and transport properties of the $\alpha - \mathcal{T}_3$ model. These are a strong dependence on the lattice parameter α and a small modification of the material parameters, related to both single electron states and collective behavior, by varying the intensity of the electron-light interaction with $\lambda_0 < 1$.

The ϕ -dependence is strongest in the graphene limit when $\phi \sim 0$, and is weak for materials whose hopping parameter is close to that for the dice lattice, i.e., satisfying $\phi \approx \pi/4$. We observe a significant increase in the plasmon damping above the Fermi level, as well as at lower energies of plasmon excitations, when α is increased from 0 to 1. The effect on the plasmon dispersion relation is particularly strong around the Fermi energy, for which the presence of the flat band in the band structure is decisive.

Once the external irradiation is applied, modification of the polarizability of a dice lattice is often opposite to that due to increasing ϕ . We see a substantial increase in a plasmon energy at a chosen wave vector, compared to a non-irradiated material. The Boltzmann conductivity, calculated in the relaxation time approximation, shows a strong decrease, once the dressing field is applied. All these results are expected to provide useful information and guidance when designing nano-electronic and nano-plasmonic devices which are based on innovative low-dimensional $\alpha - \mathcal{T}_3$ materials.

Acknowledgments

D.H. would like to acknowledge the support from the Air Force Office of Scientific Research (AFOSR). D.H is also supported by the DoD Lab-University Collaborative Initiative (LUCI) program. G.G. would like to acknowledge the support from the Air Force Research Laboratory (AFRL) through Grant #12530960.

VI. SUPPLEMENTARY INFORMATION AND MATERIALS

A. Single electronic states

The electronic states for irradiated dice lattice, pertaining to the valence and conduction bands $\gamma = \pm 1$, are obtained as

$$\Psi_d^{(C)}(\gamma, \tau | \lambda_0, \mathbf{k}) = \frac{1}{\sqrt{\mathcal{N}^{(\gamma)}}} \begin{pmatrix} \tau \mathcal{C}^{(1)} \mathbf{e}^{-i\tau\theta_{\mathbf{k}}} \\ \mathcal{C}^{(2)} \\ \tau (\hbar v_F k)^2 \mathbf{e}^{+i\tau\theta_{\mathbf{k}}} \end{pmatrix}, \quad (8)$$

where

$$\begin{aligned} \mathcal{C}^{(1)}(\gamma, \tau | \lambda_0, k) &= (\hbar v_F k)^2 + 2 \left[\Delta_{(\lambda)}^2 - 2c_0 \lambda_0 \gamma \tau \sqrt{(\hbar v_F k)^2 + \Delta_{(\lambda)}^2} \right], \\ \mathcal{C}^{(2)}(\gamma, \tau | \lambda_0, k) &= \sqrt{2} \gamma (\hbar v_F k) \left[\sqrt{(\hbar v_F k)^2 + \Delta_{(\lambda)}^2} - \gamma \tau \Delta_{(\lambda)} \right], \\ \mathcal{N}^{(\gamma)}(\tau | \lambda_0 \ll 1, k) &\simeq 2 \left\{ 2 (\hbar v_F k)^4 - 5 \gamma \tau c_0 \lambda_0 (\hbar v_F k)^3 + 9 [c_0 \lambda_0 (\hbar v_F k)]^2 + \dots \right\}. \end{aligned} \quad (9)$$

Parameter $\Delta_{(\lambda)} = 2\lambda_0 c_0 / (4 + \lambda_0^2)$ is not equivalent to the actual energy bandgap $2\Delta_0(\beta = 1, \lambda_0) = \lambda_0 c_0$. We rewrite it as

$$\Psi_d^{(E)}(\gamma, \tau | \lambda_0, \mathbf{k}) = \begin{pmatrix} \tau c_\gamma^{(1)} \mathbf{e}^{-i\tau\theta_{\mathbf{k}}} \\ c_\gamma^{(2)} \\ \tau c_\gamma^{(3)} \mathbf{e}^{+i\tau\theta_{\mathbf{k}}} \end{pmatrix}, \quad (10)$$

where for $\tau = 1$, corresponding to the K -valley, and for $\lambda_0 \ll 1$, we approximate as

$$\begin{aligned} c_\gamma^{(1)} &= \frac{\mathcal{C}^{(1)}}{\sqrt{\mathcal{N}^{(\gamma)}}}, & [c_1^{(1)}]^2 &\simeq \frac{1}{4} - \frac{1}{8} \frac{\lambda_0 c_0}{\hbar v_F k} + \dots, \\ c_\gamma^{(2)} &= \frac{\mathcal{C}^{(2)}}{\sqrt{\mathcal{N}^{(\gamma)}}}, & [c_1^{(2)}]^2 &\simeq \frac{1}{2} + \frac{3}{4} \frac{\lambda_0 c_0}{\hbar v_F k} + \dots, \\ c_\gamma^{(3)} &= \frac{(\hbar v_F k)^2}{\sqrt{\mathcal{N}^{(\gamma)}}}, & [c_1^{(3)}]^2 &\simeq \frac{1}{4} + \frac{5}{8} \frac{\lambda_0 c_0}{\hbar v_F k} + \dots. \end{aligned} \quad (11)$$

For the flat band, we obtain

$$\Psi_d^{(C)}(\gamma = 0, \tau | \lambda_0, \mathbf{k}) = \frac{1}{\sqrt{\mathcal{N}^{(0)}}} \begin{pmatrix} \tau k \mathbf{e}^{-i\tau\theta_{\mathbf{k}}} \\ 2\sqrt{2} \lambda_0 (4 - \lambda_0^2) c_0 / (\hbar v_F) \\ -\tau k \mathbf{e}^{+i\tau\theta_{\mathbf{k}}} \end{pmatrix}, \quad (12)$$

where

$$\mathcal{N}^{(0)}(\lambda_0 \ll 1, k) \simeq 2 \left[k^2 + \left(8\lambda_0 \frac{c_0}{\hbar v_F} \right)^2 \right] + \dots \quad (13)$$

The components of wave function are no longer equivalent, as expected for a finite energy gap $\Delta_0^D = \lambda_0 c_0 / 2$. This wave function could be presented as

$$\Psi_d^{(C)}(\gamma = 0, \tau | \lambda_0, \mathbf{k}) = \begin{pmatrix} c_0^{(1)} \mathbf{e}^{-i\tau\theta_{\mathbf{k}}} \\ c_0^{(2)} \\ -c_0^{(1)} \mathbf{e}^{+i\tau\theta_{\mathbf{k}}} \end{pmatrix}, \quad (14)$$

where

$$\begin{aligned} c_0^{(1)} &= \frac{k}{\sqrt{\mathcal{N}^{(0)}}}, \quad \left[c_0^{(1)} \right]^2 \simeq \frac{1}{2} - 32 \left(\frac{\lambda_0 c_0}{\hbar v_F k} \right)^2 + \dots, \\ c_0^{(2)} &= 2\sqrt{2} \lambda_0 \frac{(4 - \lambda_0^2)}{\sqrt{\mathcal{N}^{(0)}}} \frac{c_0}{\hbar v_F}, \quad \left[c_0^{(2)} \right]^2 \simeq 64 \left(\frac{\lambda_0 c_0}{\hbar v_F k} \right)^2 + \dots, \end{aligned} \quad (15)$$

B. Wavefunction overlaps

The *prefactors*, or the overlaps of states, are defined through the scalar product $\mathbb{P}_\phi(\gamma_1, \gamma_2 | \mathbf{k}, \mathbf{q})$ of the initial $\Psi_d^{(C)}(\gamma_1, \tau | \lambda_0, \mathbf{k})$ and scattered $\Psi_d^{(C)}(\gamma_2, \tau | \lambda_0, \mathbf{k}')$ electronic states with the wavevectors \mathbf{k} and $\mathbf{k}' = \mathbf{k} + \mathbf{q}$

$$\begin{aligned} \mathbb{O}_\phi\{\gamma_1, \gamma_2 | \mathbf{k}, \mathbf{q}\} &= \left| \mathbb{S}_\phi(\gamma_1, \gamma_2 | \mathbf{k}, \mathbf{q}) \right|^2, \\ \mathbb{S}_\phi(\gamma_1, \gamma_2 | \mathbf{k}, \mathbf{q}) &= \left\langle \Psi_d^{(C)}(\gamma_2, \tau | \lambda_0, \mathbf{k}') \middle| \Psi_d^{(C)}(\gamma_1, \tau | \lambda_0, \mathbf{k}) \right\rangle, \end{aligned} \quad (16)$$

where $k' = \sqrt{k^2 + q^2 + 2kq \cos(\beta_{\mathbf{k}, \mathbf{k}'})}$ and $\beta_{\mathbf{k}, \mathbf{k}'} = \theta_{\mathbf{k}'} - \theta_{\mathbf{k}}$.

For an irradiated $\lambda_0 > 0$ dice lattice with $\phi = \pi/4$ we obtain

$$\mathbb{S}_{\pi/4}\{0 \leftrightarrow +1 | \mathbf{k}, \mathbf{k}'\} = c_0^{(1)}(k') c_{+1}^{(1)}(k) \mathbf{e}^{i\tau\beta_{\mathbf{k}, \mathbf{k}'}} + c_0^{(2)}(k') c_{+1}^{(2)}(k) - c_0^{(1)}(k') c_{+1}^{(3)}(k) \mathbf{e}^{-i\tau\beta_{\mathbf{k}, \mathbf{k}'}} , \quad (17)$$

which corresponds to the transitions from the flat band $\gamma_1 = 0$ to the conduction band with $\gamma_2 = +1$, ($0 \leftrightarrow +1$ and back,

$$\mathbb{S}_{\pi/4}\{-1 \leftrightarrow +1 | \mathbf{k}, \mathbf{k}'\} = c_{-1}^{(1)}(k') c_{+1}^{(1)}(k) \mathbf{e}^{i\tau\beta_{\mathbf{k}, \mathbf{k}'}} + c_{-1}^{(2)}(k') c_{+1}^{(2)}(k) + c_{-1}^{(3)}(k') c_{+1}^{(3)}(k) \mathbf{e}^{-i\tau\beta_{\mathbf{k}, \mathbf{k}'}} \quad (18)$$

for the transitions between the valence $\gamma_1 = -1$ and conduction band with $\gamma_2 = +1$, ($-1 \leftrightarrow +1$), and finally,

$$\mathbb{S}_{\pi/4}\{+1 \leftrightarrow +1 | \mathbf{k}, \mathbf{k}'\} = c_{+1}^{(1)}(k') c_{+1}^{(1)}(k) \mathbf{e}^{i\tau\beta_{\mathbf{k}, \mathbf{k}'}} + c_{+1}^{(2)}(k') c_{+1}^{(2)}(k) + c_{+1}^{(3)}(k') c_{+1}^{(3)}(k) \mathbf{e}^{-i\tau\beta_{\mathbf{k}, \mathbf{k}'}} \quad (19)$$

We do not consider the remaining possible transitions $-1 \leftrightarrow -1$ inside the valence band and between the flat and valences bands $0 \leftrightarrow -1$, which are excluded at zero temperature for the electron doping $E_F > 0$ since all such states are completely occupied $n_F(E < 0, E_F | T = 0) = \Theta(E_F - E) \equiv 1$.

In the absence of irradiation, the prefactors are provided in Table VI C.

C. Boltzmann transport

For a finite electron doping $E_F > 0$, the inverse relaxation time is given as

$$\frac{1}{\tau(k, \lambda_0)} = \frac{n_i}{2\pi\hbar} \int_0^{2\pi} d\beta_{\mathbf{k}, \mathbf{k}'} (1 - \cos \beta_{\mathbf{k}, \mathbf{k}'}) \int_0^\infty k' dk' \left| \left\{ \int d^2\mathbf{r} \Psi(\mathbf{k}' | \mathbf{r}) U_C(\mathbf{r}) \Psi(\mathbf{k} | \mathbf{r}) \right\} / \epsilon^{(s)}(|\mathbf{k} - \mathbf{k}'|) \right|^2 \delta[\varepsilon(k) - \varepsilon(k')] , \quad (20)$$

where $\theta_{\mathbf{k}, \mathbf{k}'}$ is the angle between \mathbf{k} and \mathbf{k}' , the complete wave function is $\Psi(\mathbf{k} | \mathbf{r}) = \Psi_d(\lambda_0, \mathbf{k}) \exp[i\mathbf{k} \cdot \mathbf{r}]$. For isotropic dispersions and electronic states, corresponding to the circularly-polarized irradiation, the relaxation time depends only on $k = |\mathbf{k}|$.

In our analytical evaluation, we are going to leave out the screening factor $1/|\epsilon_s(q)|^2$. Since we are interested in a ratio of the irradiated material to that with λ_0 , we only have an error due to the change of the dielectric function. We begin with the scattering potential matrix element as

$$\mathbb{W}(\mathbf{k}, \mathbf{k}') = \int d^2\mathbf{r} \Psi(\mathbf{k}' | \mathbf{r}) U_C(\mathbf{r}) \Psi(\mathbf{k} | \mathbf{r}). \quad (21)$$

The scattering potential is equivalent to the Coulomb interaction with a charged impurity Q : $U_C(r) = eQ/(4\pi\epsilon_0 r) = \alpha_C/r$. The inverse relaxation time is given as

$$\mathbb{W}(\mathbf{k}, \mathbf{k}') = \frac{\alpha_C}{2} \mathbb{O}(\mathbf{k}, \mathbf{k}') \int d^2\mathbf{r} \exp[i(\mathbf{k} - \mathbf{k}') \cdot \mathbf{r}] / r. \quad (22)$$

where $\mathbb{O}(\mathbf{k}, \mathbf{k}')$ is the overlap in the conduction band, defined in Eq. (19).

$$U_C(q) = \alpha_C \int d^2\mathbf{r} \frac{\exp[i(\mathbf{k} - \mathbf{k}') \cdot \mathbf{r}]}{r} = \frac{2\pi \alpha_C}{|\mathbf{k} - \mathbf{k}'|}. \quad (23)$$

Indeed, $(\mathbf{k} - \mathbf{k}') \cdot \mathbf{r} = \Delta\mathbf{k} \cdot \mathbf{r} = \Delta k_x x + \Delta k_y y = \Delta k_x r \cos \theta + \Delta k_y r \sin \theta$. Substituting $\xi(\theta) = \Delta k_x \cos \theta + \Delta k_y \sin \theta$ and making use of the following identity

$$\int_{-\infty}^{\infty} e^{i\xi r} dr = 2\pi\delta(\xi), \quad (24)$$

we obtain

$$U_C(k, k') = 2\pi \alpha_C \int_0^{2\pi} d\theta \delta[\xi(\theta)] = 2\pi \alpha_C (\Delta k_x^2 + \Delta k_y^2)^{-1/2} = \frac{2\pi \alpha_C}{|\mathbf{k} - \mathbf{k}'|}. \quad (25)$$

Transition rate in the Born approximation

$$\mathbb{T}(k, \beta_{\mathbf{k}', \mathbf{k}'}) = \frac{2\pi}{\hbar} \left| \mathbb{W}^{\gamma, \gamma'}(\mathbf{k}, \mathbf{k}') \right|^2 \delta[\varepsilon(k) - \varepsilon(k')] \quad (26)$$

Since the electron states, corresponding to \mathbf{k} and \mathbf{k}' momenta have identical energy gaps, the condition $\varepsilon(|\mathbf{k}|) = \varepsilon(|\mathbf{k}'|)$ is equivalent to $k' = k$ and

$$\begin{aligned} \delta[\varepsilon(k) - \varepsilon(k')] &= \frac{1}{\hbar v_F} \delta(k - k'), \\ |\mathbf{k} - \mathbf{k}'| &= 2k \sin\left(\frac{\beta_{\mathbf{k}, \mathbf{k}'}}{2}\right), \end{aligned} \quad (27)$$

which eliminates the radial component of k -integral.

The inverse relaxation time

$$\frac{1}{\tau_\phi(\mathbf{k})} = \frac{n_i}{(2\pi)^2} \int_0^{2\pi} d\beta (1 - \cos \beta) \int_0^\infty k' dk' \mathbb{T}(\mathbf{k}, \mathbf{k}'), \quad (28)$$

where $\theta_{\mathbf{k}, \mathbf{k}'}$ is the angle between \mathbf{k} and \mathbf{k}' .

$$\begin{aligned} \frac{1}{\tau(\lambda_0, k)} &= \frac{\pi n_i}{2v_F} \left(\frac{\alpha_C}{\hbar}\right)^2 \frac{1}{k} \mathbb{I}(\lambda_0), \\ \mathbb{I}(\lambda_0) &= \int_0^{2\pi} d\beta_{\mathbf{k}, \mathbf{k}'} \{ [c_1(\lambda_0, k) + c_3(\lambda_0, k)] \cos \beta_{\mathbf{k}, \mathbf{k}'} + c_2(\lambda_0, k) \}^2 - \{ [c_1(\lambda_0, k) - c_3(\lambda_0, k)] \sin \beta_{\mathbf{k}, \mathbf{k}'} \}^2. \end{aligned} \quad (29)$$

Material	Overlap	Inverse relaxation time
Graphene	$(1 + \cos \beta_{\mathbf{k},\mathbf{k}'})/2$	π
Dice lattice	$(1 + \cos \beta_{\mathbf{k},\mathbf{k}'})^2/4$	$3\pi/4$
$\alpha - \mathcal{T}_3$	$1/4 \{ (1 + \cos \beta_{\mathbf{k},\mathbf{k}'})^2 + \cos^2(2\phi) \sin^2 \beta_{\mathbf{k},\mathbf{k}'} \}$	$\pi/8 \{ 7 + \cos(4\phi) \}$

TABLE I: Prefactors (wavefunction overlaps), and inverse relaxation time $\mathbb{I}(\lambda_0)$ factor from Eq. (29) for graphene and general $\alpha - \mathcal{T}_3$ materials in the absence of external irradiation.

Finally, the current components are

$$j^{(i)} = \left(\frac{e}{\pi} \right)^2 \int d^2\mathbf{k} \left[\mathcal{E}_0 v^{(i)}(\mathbf{k}) \right] \tau_\phi(\mathbf{k}) v^{(i)}(\mathbf{k}) \left\{ - \frac{\partial f[\varepsilon(k) | \mu(T), T]}{\partial \varepsilon(k)} \right\}. \quad (30)$$

At $T = 0$, we simplify $-\partial f[\varepsilon(k) | \mu(T), T]/\partial \varepsilon(k)$ as $\delta[\varepsilon(k) - E_F]$, and for a isotropic energy dispersions no integration is needed.

-
- ¹ A. Raoux, M. Morigi, J.-N. Fuchs, F. Piéchon, and G. Montambaux, Physical review letters **112**, 026402 (2014).
 - ² J. Vidal, R. Mosseri, and B. Douçot, Physical review letters **81**, 5888 (1998).
 - ³ M. Vigh, L. Oroszlány, S. Vajna, P. San-Jose, G. Dávid, J. Cserti, and B. Dóra, Physical Review B **88**, 161413 (2013).
 - ⁴ M. Rizzi, V. Cataudella, and R. Fazio, Physical Review B **73**, 144511 (2006).
 - ⁵ K. Novoselov, A. K. Geim, S. Morozov, D. Jiang, M. Katsnelson, I. Grigorieva, S. Dubonos, and A. Firsov, nature **438**, 197 (2005).
 - ⁶ D. Leykam, A. Andreanov, and S. Flach, Advances in Physics: X **3**, 1473052 (2018).
 - ⁷ J. D. Malcolm and E. J. Nicol, Physical Review B **93**, 165433 (2016).
 - ⁸ J. Romhányi, K. Penc, and R. Ganesh, Nature communications **6**, 6805 (2015).
 - ⁹ X. Huang, Y. Lai, Z. H. Hang, H. Zheng, and C. Chan, Nature materials **10**, 582 (2011).
 - ¹⁰ Y. Li, S. Kita, P. Muñoz, O. Reshef, D. I. Vulis, M. Yin, M. Lončar, and E. Mazur, Nature Photonics **9**, 738 (2015).
 - ¹¹ R. A. Vicencio, C. Cantillano, L. Morales-Inostroza, B. Real, C. Mejía-Cortés, S. Weimann, A. Szameit, and M. I. Molina, Physical review letters **114**, 245503 (2015).
 - ¹² S. Mukherjee, A. Spracklen, D. Choudhury, N. Goldman, P. Öhberg, E. Andersson, and R. R. Thomson, Physical review letters **114**, 245504 (2015).
 - ¹³ E. Illes, Ph.D. thesis (2017).
 - ¹⁴ E. Illes and E. Nicol, Physical Review B **94**, 125435 (2016).
 - ¹⁵ E. Illes, J. P. Carbotte, and E. J. Nicol, Phys. Rev. B **92**, 245410 (2015).
 - ¹⁶ B. Dey and T. K. Ghosh, Physical Review B **98**, 075422 (2018).
 - ¹⁷ B. Dey and T. K. Ghosh, arXiv preprint arXiv:1901.10778 (2019).
 - ¹⁸ T. Biswas and T. K. Ghosh, Journal of Physics: Condensed Matter **30**, 075301 (2018).
 - ¹⁹ T. Biswas and T. K. Ghosh, Journal of Physics: Condensed Matter **28**, 495302 (2016).
 - ²⁰ F. Piéchon, J. Fuchs, A. Raoux, and G. Montambaux, in *Journal of Physics: Conference Series* (IOP Publishing, 2015), vol. 603, p. 012001.
 - ²¹ C. J. Tabert and E. J. Nicol, Physical Review B **89**, 195410 (2014).
 - ²² M. Katsnelson, K. Novoselov, and A. Geim, Nature physics **2**, 620 (2006).
 - ²³ E. Illes and E. Nicol, Physical Review B **95**, 235432 (2017).
 - ²⁴ G. Gumbs, A. Iurov, D. Huang, and L. Zhemchuzhna, Physical Review B **89**, 241407 (2014).
 - ²⁵ E. Gorbar, V. Gusynin, and D. Oriekhov, Physical Review B **99**, 155124 (2019).
 - ²⁶ P. Perez-Piskunow, G. Usaj, C. Balseiro, and L. F. Torres, Physical Review B **89**, 121401 (2014).
 - ²⁷ H. L. Calvo, H. M. Pastawski, S. Roche, and L. E. F. Torres, Applied Physics Letters **98**, 232103 (2011).
 - ²⁸ E. S. Morell and L. E. F. Torres, Physical Review B **86**, 125449 (2012).
 - ²⁹ Z. Gu, H. Fertig, D. P. Arovas, and A. Auerbach, Physical review letters **107**, 216601 (2011).
 - ³⁰ V. Dal Lago, E. S. Morell, and L. F. Torres, Physical Review B **96**, 235409 (2017).
 - ³¹ G. Usaj, P. Perez-Piskunow, L. F. Torres, and C. Balseiro, Physical Review B **90**, 115423 (2014).
 - ³² I. Iorsh, K. Dini, O. Kibis, and I. Shelykh, Physical Review B **96**, 155432 (2017).
 - ³³ N. Goldman and J. Dalibard, Physical review X **4**, 031027 (2014).
 - ³⁴ O. Kibis, Physical Review B **81**, 165433 (2010).
 - ³⁵ A. Iurov, G. Gumbs, O. Roslyak, and D. Huang, Journal of Physics: Condensed Matter **24**, 015303 (2011).
 - ³⁶ O. Kibis, K. Dini, I. Iorsh, and I. Shelykh, Physical Review B **95**, 125401 (2017).
 - ³⁷ O. Kibis, K. Dini, I. Iorsh, and I. Shelykh, Semiconductors **52**, 523 (2018).

- ³⁸ O. Kyriienko, O. Kibis, and I. Shelykh, *Physical Review B* **99**, 115411 (2019).
- ³⁹ A. Iurov, G. Gumbs, D. Huang, and L. Zhemchuzhna, *Journal of Applied Physics* **121**, 084306 (2017).
- ⁴⁰ A. Iurov, G. Gumbs, and D. Huang, *Journal of Modern Optics* **64**, 913 (2017).
- ⁴¹ S. Morina, K. Dini, I. V. Iorsh, and I. A. Shelykh, *ACS Photonics* **5**, 1171 (2018).
- ⁴² S. Morina, O. V. Kibis, A. A. Pervishko, and I. A. Shelykh, *Phys. Rev. B* **91**, 155312 (2015).
- ⁴³ K. Kristinsson, O. Kibis, S. Morina, and I. Shelykh, *Scientific reports* **6**, 20082 (2016).
- ⁴⁴ P. Pyatkovskiy, *Journal of Physics: Condensed Matter* **21**, 025506 (2008).
- ⁴⁵ A. Iurov, L. Zhemchuzhna, G. Gumbs, and D. Huang, *Journal of Applied Physics* **122**, 124301 (2017).
- ⁴⁶ A. Iurov, G. Gumbs, and D. Huang, *arXiv preprint arXiv:1806.09172* (2018).
- ⁴⁷ V. Kozin, I. Iorsh, O. Kibis, and I. Shelykh, *Physical Review B* **97**, 035416 (2018).
- ⁴⁸ A. Politano and G. Chiarello, *Nanoscale* **6**, 10927 (2014).
- ⁴⁹ B. Wunsch, T. Stauber, F. Sols, and F. Guinea, *New Journal of Physics* **8**, 318 (2006).
- ⁵⁰ A. Scholz, T. Stauber, and J. Schliemann, *Physical Review B* **88**, 035135 (2013).
- ⁵¹ G. Gumbs, A. Balassis, A. Iurov, and P. Fekete, *The Scientific World Journal* **2014** (2014).
- ⁵² J. Tempere, I. F. Silvera, and J. T. Devreese, *Phys. Rev. B* **65**, 195418 (2002).
- ⁵³ A. Iurov, G. Gumbs, B. Gao, and D. Huang, *Applied Physics Letters* **104**, 203103 (2014).
- ⁵⁴ D. Huang, A. Iurov, H.-Y. Xu, Y.-C. Lai, and G. Gumbs, *arXiv preprint arXiv:1903.07795* (2019).
- ⁵⁵ A. Iurov, G. Gumbs, and D. Huang, *Physical Review B* **98**, 075414 (2018).
- ⁵⁶ L. A. Falkovsky and S. S. Pershoguba, *Phys. Rev. B* **76**, 153410 (2007).
- ⁵⁷ T. Ando, A. B. Fowler, and F. Stern, *Reviews of Modern Physics* **54**, 437 (1982).
- ⁵⁸ E. Hwang and S. D. Sarma, *Physical Review B* **79**, 165404 (2009).
- ⁵⁹ A. C. Neto, F. Guinea, N. M. Peres, K. S. Novoselov, and A. K. Geim, *Reviews of modern physics* **81**, 109 (2009).
- ⁶⁰ E. H. Hwang and S. Das Sarma, *Phys. Rev. B* **77**, 195412 (2008).
- ⁶¹ M. Rizzi, V. Cataudella, and R. Fazio, *Physical Review B* **73**, 144511 (2006).